Site preference of ternary Fe addition in $Ni_{75}Al_{25}$

2003 J. Phys.: Condens. Matter 15 4903

(http://iopscience.iop.org/0953-8984/15/29/302)

INSTITUTE OF PHYSICS PUBLISHING JOURNAL OF PHYSICS: CONDENSED MATTER

J. Phys.: Condens. Matter **15** (2003) 4903–4918 PII: S0953-8984(03)60455-8

Site preference of ternary Fe addition in $Ni_{75}Al_{25}$

B Annie D'Santhoshini and S N Kaul[1]

School of Physics, University of Hyderabad, Central University PO, Hyderabad 500 046, Andhra Pradesh, India

E-mail: kaulsp@uohyd.ernet.in

Received 6 March 2003, in final form 6 June 2003
Published 11 July 2003
Online at stacks.iop.org/JPhysCM/15/4903

Abstract

An extensive investigation of structure, surface morphology and composition in $Ni_{75-x}Fe_xAl_{25}$ alloys with nominal composition $x = 0$, 5, 10 and 20, deliberately 'prepared' in different states of site disorder, has been carried out by x-ray diffraction, scanning electron microscopy, x-ray fluorescence (energy dispersive absorption of x-rays) and inductively coupled plasma optical emission spectroscopy. The results of an elaborate analysis of the present x-ray diffraction data on $Ni_{75-x}Fe_xAl_{25}$ (Ni-deficit) alloys and those reported previously on $Ni_{75}Al_{25-x}Fe_x$ (Al-deficit) alloys vindicate the recent theoretical prediction that the composition of the alloy plays a decisive role in determining the site preference of Fe by clearly demonstrating that Fe has nearly *exclusive* Ni (Al) site preference in the Ni-deficit (Al-deficit) alloys and thereby resolves a long-standing controversy surrounding the site preference of the ternary Fe addition in the γ'-Ni_3Al phase in the Ni–Al phase diagram. However, contrary to the recent theoretical claim that entropy promotes Al site preference of Fe in Ni-deficit alloys, we find that Fe exclusively occupies the Ni sites in those Ni-deficit alloys that have a greater degree of site disorder.

1. Introduction

Owing to their attractive high-temperature properties, a number of binary intermetallic compounds were considered to be promising materials for the development of new catalysts or superalloys for the aircraft industry. However, low ductility at ambient temperature and a tendency to fracture proved to be the main stumbling blocks for such practical applications. This obstacle has been subsequently overcome in some compounds by the addition of substitutional elements that result in a significant improvement in mechanical properties. The γ' phase in the Ni–Al phase diagram is one such compound. The γ'-Ni_3Al phase crystallizes

[1] Author to whom any correspondence should be addressed.

0953-8984/03/294903+16$30.00

in a cubic structure of $L1_2$ type (Cu_3Au prototype). In the completely ordered compound, Ni and Al atoms respectively occupy face centres and corner sites of a face-centred cubic (fcc) unit cell. The corner sites and face-centred sites thus form two separate but interpenetrating Al and Ni sublattices. A substitutional ternary species may exclusively occupy the Ni sites, Al sites or may occupy both Ni and Al sites with no site preference at all. A strong correlation between the site occupation of the ternary additions and the mechanical properties of the γ' phase has been established in a number of previous works (Rawlings and Staton-Bevan 1975, Suzuki *et al* 1980, Inoue *et al* 1983, Pope and Ezz 1984, Liu *et al* 1985, Takasugi and Izumi 1985). Recently enhanced ductility has been observed (Chiba *et al* 1990, 1991a, 1991b) when the ternary addition *preferentially* substitutes Ni on the face-centred sites in Ni_3Al. Thus, a complete knowledge about the site occupation of the substitutional ternary species is crucial to understanding the mechanism of improvement in the mechanical properties by such additions.

The site preference of ternary additions in γ'-Ni_3Al has been extensively investigated both experimentally (Kriege and Baris 1969, Karg *et al* 1971, Loomis *et al* 1972, Nicholls and Rawlings 1977, Blavette and Bostel 1984, Miller and Bentley 1986, Miller and Horton 1987, Bohn *et al* 1987a, 1987b, Lin *et al* 1987, Shindo *et al* 1988, Lin and Pope 1990, Marty *et al* 1990, Munroe and Baker 1991, Chiba *et al* 1991, Hono *et al* 1992, Numakura *et al* 1993, Pascarelli *et al* 1994) and theoretically (Machlin and Shao 1977, Ochiai *et al* 1984, Xu *et al* 1987, Wu *et al* 1989, Enomoto and Harada 1989, Marty *et al* 1991, Wolverton and de Fontaine 1994, Sluiter and Kawazoe 1995, Ruban and Skriver 1997, Lawniczak-Jablonska *et al* 2000). As a result of these efforts, Ni (Al) sublattice preference is now well established in the case of Co, Cu and Pd (Ti, V and Nb). For Fe, however, contradictory results have been obtained. Mössbauer spectroscopy (Nicholls and Rawlings 1977) has indicated a weak, composition-dependent, preference for the Al sublattice. Channeling-enhanced microanalysis (Shindo *et al* 1988) revealed no discernible site preference while a recent K-edge extended x-ray absorption fine structure (Pascarelli *et al* 1994) and Lα emission and absorption x-ray spectroscopy (Lawniczak-Jablonska *et al* 2000) studies concluded that Fe has an almost exclusive site preference for the Al sublattice. At this stage, it is worth noting that the last two x-ray investigations have been carried out on Al-deficit (with respect to the stoichiometric composition, $Ni_{75}Al_{25}$) alloys and hence such studies, at best, establish that Fe does not have a strong site preference for the Ni sublattice for Al-poor alloys. Based on an analysis of extracted precipitates, Kriege and Baris 1969 concluded that Fe has a strong preference for the Ni sites but this conclusion has been questioned (Rawlings and Staton-Bevan 1975) later. Similarly, the theoretical opinion on the issue of site preference of Fe is sharply divided; for details, see Ruban and Skriver (1997). This subject assumes great importance primarily because Fe addition has a drastic influence on the mechanical, electrical and magnetic properties of γ'-Ni_3Al.

Taking cognizance of the fact that most of the previous experimental investigations have focused on Al-deficit Fe-substituted Ni_3Al alloys alone and such studies are incapable of revealing strong Ni-site preference, if any, we have undertaken a systematic structural, magnetic and electrical resistivity study of Ni-deficit (with respect to the stoichiometric composition, $Ni_{75}Al_{25}$) alloys with nominal composition $Ni_{70}Fe_5Al_{25}$, $Ni_{65}Fe_{10}Al_{25}$ and $Ni_{55}Fe_{20}Al_{25}$. In view of the theoretical prediction (Ruban and Skriver 1997) that both composition and temperature strongly influence the site substitution behaviour of the ternary additions, prior to the measurements, different samples of a given alloy composition have been subjected to different heat treatments so as to 'prepare' them in different states of site disorder. Such a study permits one to ascertain if the thermal history of the sample has any effect on the site preference of Fe. The present paper deals exclusively with the structural aspects, while the influence of Fe substitution on magnetic and transport properties of γ'-Ni_3Al will form the subject of forthcoming papers.

Table 1. Nominal and actual composition of the samples.

	Nominal composition			Actual composition		
Sample	Ni	Fe	Al	Ni	Fe	Al
$Ni_{75}Al_{25}$	75.00	0.00	25.00	75.14(17)	0.0	24.86(9)
$Ni_{70}Fe_5Al_{25}$	70.00	5.00	25.00	71.19(17)	3.35(5)	25.46(19)
$Ni_{65}Fe_{10}Al_{25}$	65.00	10.00	25.00	65.06(17)	10.04(9)	24.90(19)
$Ni_{55}Fe_{20}Al_{25}$	55.00	20.00	25.00	55.01(14)	20.05(13)	24.94(19)

2. Sample preparation and characterization

Ultra-high purity (99.999%) nickel, iron and aluminium were taken in stoichiometric proportions by weight and melted in an alumina crucible using radio-frequency (RF) induction heating. The melt was kept in the crucible for a couple of minutes for homogenization and then poured into a cylindrical hole in a massive copper mould. The entire operation from melting to pouring was carried out under argon gas (of 99.999% purity) pressure of >1 atm. Polycrystalline samples with nominal composition $Ni_{75}Al_{25}$, $Ni_{70}Fe_5Al_{25}$, $Ni_{65}Fe_{10}Al_{25}$ and $Ni_{55}Fe_{20}Al_{25}$ (denoted for brevity as Fe_0, Fe_5, Fe_{10} and Fe_{20}, respectively) were thus prepared in the form of rods of dimensions 10 mm in diameter and 100 mm in length. Rectangular parallelepipeds of dimensions $40 \times 2.5 \times 0.5$ mm^3 and discs of 10 mm diameter and 5 mm thickness, spark-cut from the rods, are henceforth referred to as the 'as-prepared' samples. Two rectangular strips of a given composition were annealed at 520 °C for 16 days in a quartz tube evacuated to a pressure of 10^{-7} Torr and subsequently water-quenched. The so-called 'annealed' samples were thus prepared.

A portion of the 'as-prepared' polycrystalline rods was melt-quenched to form ribbons. In this preparation process, the molten alloy, contained in a quartz tube of 5 mm inner diameter, is ejected (at a temperature of 1500 °C and helium pressure of 200 mbar) out in the form of a jet through a rectangular slit of dimensions 3.2×0.49 mm^2 on one end of the quartz tube onto a rotating copper wheel of diameter 200 mm. The tangential velocity of the wheel, maintained at a temperature of 22 °C, was 30 m s^{-1}. Long thin ribbons of width 2 mm and thickness $\sim$30 μm are thus formed when the melt comes in contact with the copper wheel. The samples so produced are labelled as the 'quenched' samples.

So far as the mechanical strength of the alloys in question is concerned, the following observations were made. For a given alloy composition, brittleness *increases* in the *sequence* 'annealed' $\rightarrow$ 'as-prepared' $\rightarrow$ 'quenched'. Among the samples prepared by a given technique ('as-prepared' or 'quenched' or 'annealed'), brittleness decreases drastically with increasing Fe concentration.

The chemical composition of the samples was determined by x-ray fluorescence and inductively coupled plasma optical emission spectroscopy. The actual chemical composition of these samples is compared with the nominal composition in table 1. From the entries in table 1, it is evident that the actual composition deviates significantly from the nominal one only in the case of the $Ni_{70}Fe_5Al_{25}$ alloy.

3. Results and discussion

Extensive x-ray diffraction measurements, using Cu Kα radiation, have been performed on the 'as-prepared', 'annealed' and 'quenched' samples (in the form of discs, rectangular strips and ribbons, respectively) at room temperature over the angle, 2θ, range of $10^\circ \leqslant 2\theta \leqslant 100^\circ$. Figures 1–3 compare the diffraction patterns obtained on the samples of different compositions

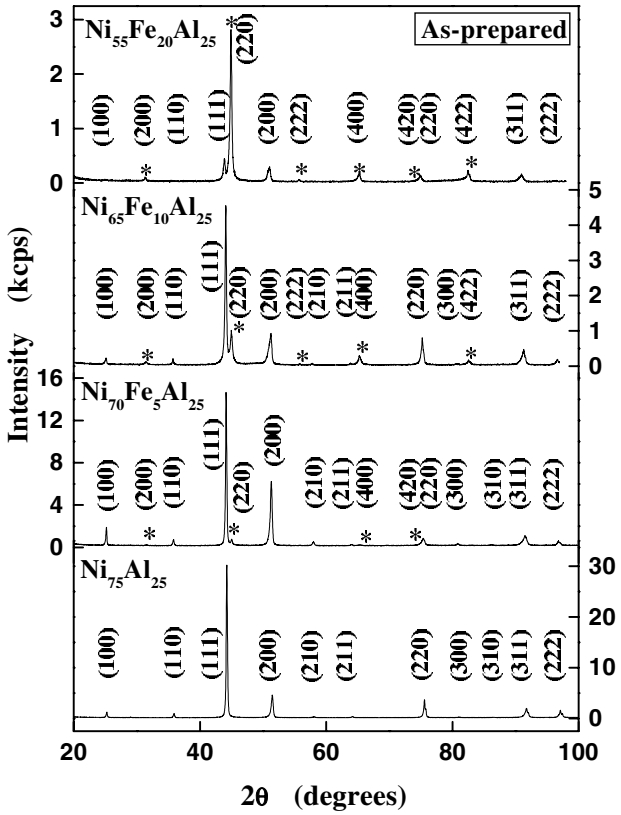

Figure 1. X-ray diffraction patterns for the 'as-prepared' (see the text) samples. The peaks with and without an asterisk correspond to the Fe_3Al and Ni_3Al phases, respectively.

but with the same thermal history while figures 4–7 serve to highlight the changes in the Bragg diffraction patterns of a sample of given composition brought about by different preparation conditions. All the observed Bragg peaks, including the weakest reflections, could be completely indexed on the basis of either the Cu_3Au type $L1_2$ structure (Ni_3Al phase) or the DO_3 structure (Fe_3Al phase) or both, as is evident from these figures. The salient features that the Bragg diffraction patterns, shown in figures 1–7, present are as follows.

(i) Regardless of the method of preparation (and hence the sample thermal history), the nucleation of the Fe_3Al phase occurs at Fe concentrations as low as 3 at.%, clearly apparent in the case of 'as-prepared' and 'quenched' Fe_5 samples, and this phase grows at the expense of the Ni_3Al phase as the Fe concentration increases beyond 3 at.% (figures 1–3) so much so that the Ni_3Al phase is relegated to a minor phase in the 'quenched' Fe_{20} sample.

(ii) In the 'quenched' state, diffraction patterns for the samples Fe_0 and Fe_5 consist of *satellite* (s) peaks of *lower* intensity at *higher* Bragg angles, θ_B^s, and *main* (m) Bragg peaks of *higher* intensity at *lower* angles, θ_B^m (clearly visible in the case of Fe_0 in figures 3 and 4) such that $\theta_B^s - \theta_B^m \equiv \phi = 0.29(1)^\circ$ and $0.11(1)^\circ$ for Fe_0 (Semwal and Kaul 2002) and Fe_5, respectively; at higher Fe concentrations, the satellite peaks are completely suppressed and only the main peaks occur. The splitting of the main as well as the satellite (220)

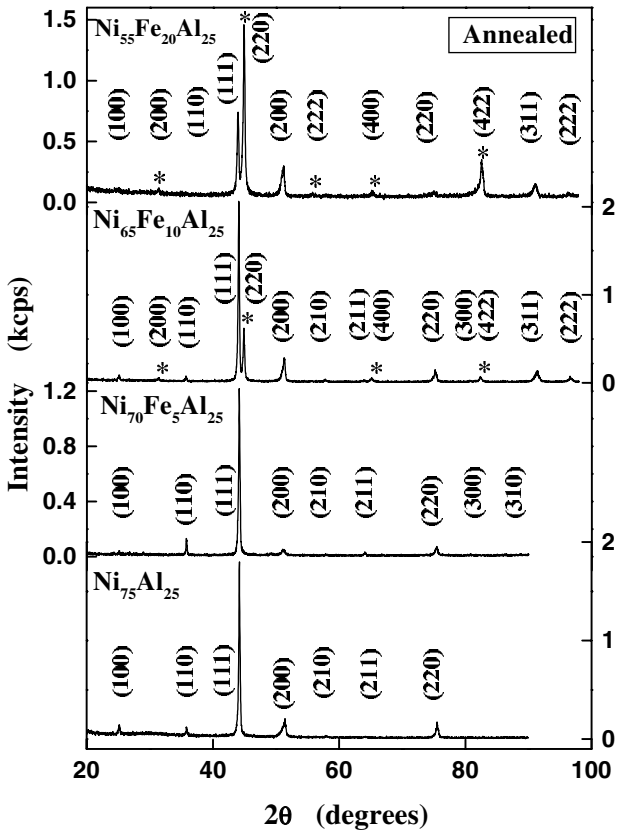

Figure 2. X-ray diffraction patterns for the 'annealed' (see the text) samples. The peaks with and without an asterisk correspond to the Fe_3Al and Ni_3Al phases, respectively.

peaks into $K\alpha_1$ and $K\alpha_2$ components is also evident from the x-ray diffraction pattern for the quenched Fe_0 sample (figure 4).

(iii) A comparison of the Fe-containing 'as-prepared' samples with their annealed counterparts reveals that *annealing promotes* the *growth* of the Ni_3Al phase *at the cost of the* Fe_3Al phase.

(iv) Barring the Fe_0 sample, annealing suppresses to a large extent the (200) texture present in the 'as-prepared' and 'quenched' samples.

(v) The splitting of Bragg peaks into main and satellite peaks in 'quenched' Fe_0 and Fe_5 samples is *absent* in their 'as-prepared' and 'annealed' counterparts (figures 4 and 5).

(vi) In sharp contrast with the Ni_3Al phase, which is characterized by the presence of both *fundamental* (*F*) (111), (200), (220), (311), (222). . . and *superstructure* (*S*) (100), (110), (210), (211), (300), (310), . . . Bragg reflection peaks, the Fe_3Al phase manifests itself in *only* the fundamental reflections, (200), (220), (222), (400), (331), (422), . . . (figures 4–7). In the quenched Fe_{20} sample, *only* an extremely weak (100) superstructure peak of Ni_3Al accompanies the fundamental reflections corresponding to the Fe_3Al and Ni_3Al phases (figure 7).

Figure 8 displays the scanning electron micrographs taken on samples with Fe concentration $x = 0$ and 20. These micrographs are representative of those for the remaining

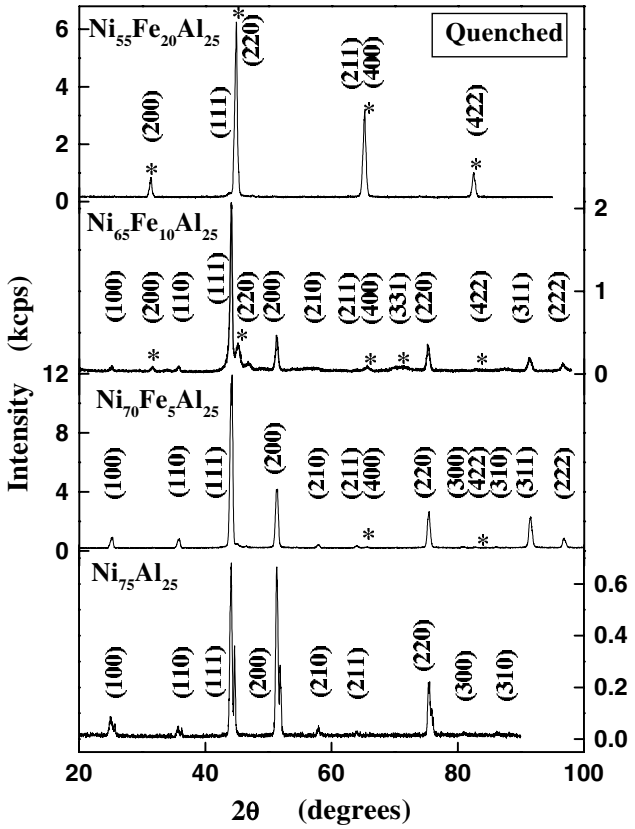

Figure 3. X-ray diffraction patterns for the 'quenched' (see the text) samples. The peaks with and without an asterisk correspond to the Fe_3Al and Ni_3Al phases, respectively.

compositions as well. A close scrutiny of these micrographs using the EDAX (energy dispersive absorption of x-rays) technique reveals the following. Barring the Fe_5 samples, the 'as-prepared' and 'quenched' Fe_{10} and Fe_{20} samples show a significant variation, particularly in the Fe concentration (x), from the lighter to darker regions in the scanning electron micrographs and this dispersion in the x values *increases* with Fe concentration. By contrast, the 'annealed' counterparts exhibit hardly any variation in composition (within the error limits) from one portion of the sample to the other. These observations thus lend a firm support to the above-mentioned findings (i) and (iii), based on the x-ray diffraction data.

The occurrence of satellite peaks in quenched Fe_0 and Fe_5 samples basically reflects the existence of two fcc lattices of different interplanar spacings d_m and d_s, corresponding to the main and satellite reflections. The *interplanar* spacings d_m and d_s are related through the expression $(1/d_s) = (1/d_m) + \phi\sqrt{(2/\lambda)^2 - (1/d_m)^2}$ or, alternatively, by $d_s = d_m/(1 + \phi \cot\theta_B^m)$, where λ is the wavelength of the incident x-ray radiation. The most refined values of the interatomic spacings (lattice parameter a) for the interpenetrating fcc lattices that give rise to main and satellite reflections in the quenched samples Fe_0 and Fe_5, are obtained by the well-known Nelson–Riley–Taylor–Sinclair method (Nelson and Riley 1945, Taylor and Sinclair 1945). The same method is used to arrive at accurate values of a for the remaining samples from the Bragg reflections, corresponding to the Ni_3Al phase. The distance $r_{nn} = a/\sqrt{2}$ between the nearest neighbours, computed from the values of the lattice

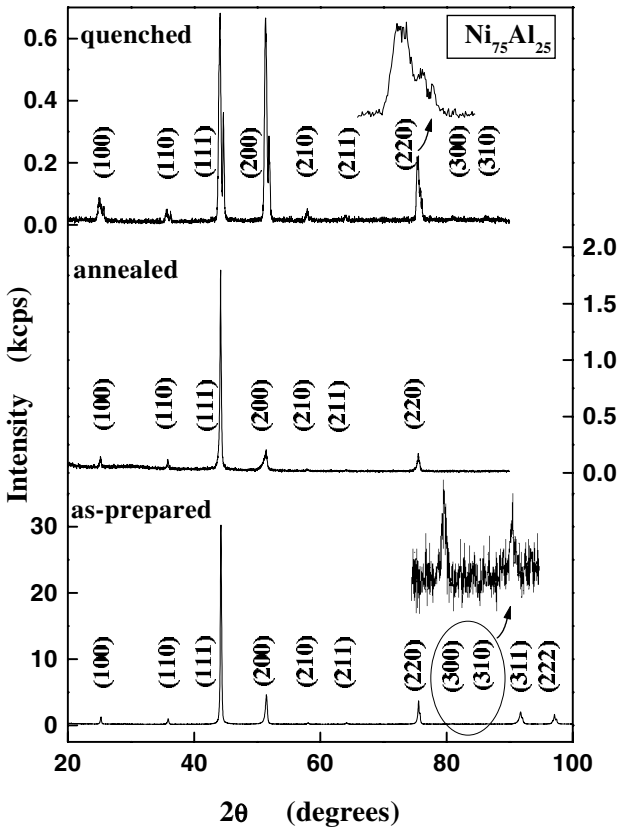

Figure 4. X-ray diffraction patterns for $Ni_{75}Al_{25}$ samples with different thermal histories (see the text). An enlarged view of the (220) peak in a 'quenched' $Ni_{75}Al_{25}$ sample and (300), (310) peaks in an 'as-prepared' $Ni_{75}Al_{25}$ sample is also presented in this figure to highlight certain features of such peaks or the existence of the weak intensity peaks in question.

parameter, a, is plotted against Fe concentration, x, in figure 9. Regardless of the sample thermal history, r_{nn} is found to increase *linearly* with x. However, the rate of increase of r_{nn} with x slows down in the sequence 'as-prepared' $\rightarrow$ 'quenched' $\rightarrow$ 'annealed'. Similar data on Al-deficit alloys, where Ni concentration is fixed at 75 at.% and Fe concentration varies at the expense of Al concentration, i.e. $Ni_{75}Al_{25-x}Fe_x$, reported (Pascarelli *et al* 1994) previously, have also been included in figure 9 for comparison. In sharp contrast with the *linear increase* in r_{nn} with x in Ni-deficit alloys where Al concentration is held constant at 25 at.% and Fe concentration varies at the cost of Ni concentration, i.e. the present case, r_{nn} *decreases linearly* with x in Al-deficit alloys.

In an attempt to understanding the contrasting behaviours of $r_{nn}(x)$ in Ni- and Al-deficit γ'-phase alloys, we consider the effect of atomic size explicitly and treat other relevant factors, such as the electronic structure of the ternary addition, only indirectly. To this end, the values of ionic radii $r_i^{Fe} = 1.27$ Å, $r_i^{Ni} = 1.245$ Å and $r_i^{Al} = 1.306$ Å (1.31 Å) of Fe, Ni and Al in close-packed structures are used to compute twice the *average* ionic radius, $2\langle r_i \rangle$ (which is a direct measure of the nearest-neighbour interatomic distance, r_{nn}) for the following possibilities of site occupation of the ternary Fe addition in Ni-deficit (Al-deficit) alloys from the relation $2\langle r_i \rangle = 2[c_{Ni}r_i^{Ni} + c_{Fe}r_i^{Fe} + c_{Al}r_i^{Al}]$, where c_{Ni}, c_{Fe} and c_{Al} are the fraction of Ni, Fe and Al

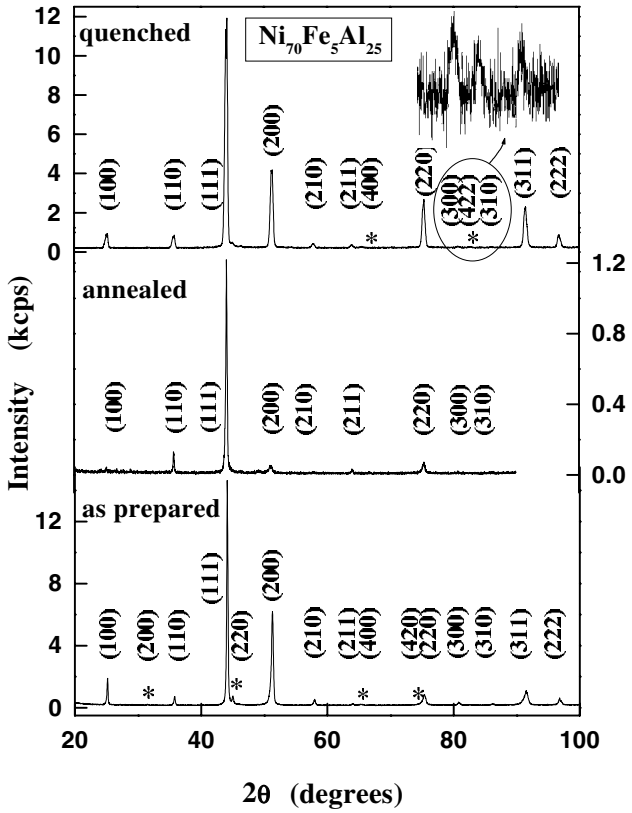

Figure 5. X-ray diffraction patterns for $Ni_{70}Fe_5Al_{25}$ samples with different thermal histories (see the text). This figure also presents an enlarged view of the (300), (422) and (310) peaks of very weak intensity in the case of a 'quenched' $Ni_{70}Fe_5Al_{25}$ sample. The peaks with and without an asterisk correspond to the Fe_3Al and Ni_3Al phases, respectively.

atoms on the Ni, Ni and/or Al and Al sites, respectively, such that $c_{Ni} + c_{Fe} + c_{Al} = 1$. In these calculations, the parent intermetallic compound Ni_3Al is assumed to be in a *completely ordered* state (i.e. Ni and Al atoms respectively occupy face centres and corners of the fcc unit cell in this compound) and instead of using the reported value $r_i^{Al} = 1.43$ Å (as is the case for r_i^{Fe} and r_i^{Ni}), the value of r_i^{Al} is chosen such that the computed value of $2\langle r_i \rangle$ *equals* the observed value (this work and Pascarelli *et al* 1994) of r_{nn} for Ni_3Al. Note that the actual charge distribution around an ion is approximated by an *effective spherical* charge distribution and hence the ionic radii refer to the radii of such effective charged spheres (i.e. the ions). The following cases of site occupation have been considered.

- Case I: Fe atoms exclusively occupy the *empty* Ni sites.
- Case II: Fe atoms are equally distributed among Ni and Al sites and the Al atoms displaced by Fe atoms from the Al sites occupy Ni sites.
- Case III: Fe atoms exclusively occupy Al sites and the Al atoms displaced from the Al sites occupy the Ni sites.
- Case IV: Fe atoms have exclusive Al-site preference and occupy empty Al sites.
- Case V: 75% (25%) of Fe atoms occupy Al (Ni) sites and the displaced Ni atoms occupy Al sites.

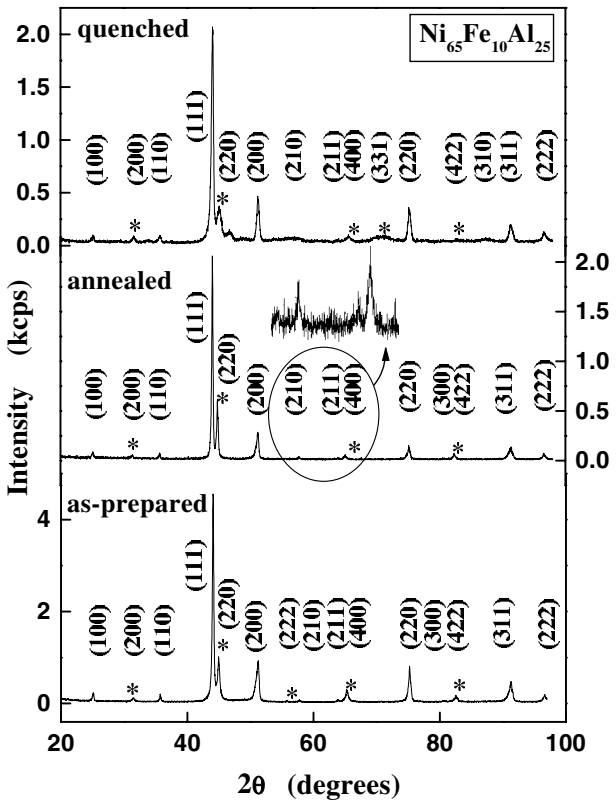

Figure 6. X-ray diffraction patterns for $Ni_{65}Fe_{10}Al_{25}$ samples with different thermal histories (see the text). This figure also presents an enlarged view of the (210), (211) and (400) peaks of very weak intensity in the case of an 'annealed' $Ni_{65}Fe_{10}Al_{25}$ sample. The peaks with and without an asterisk correspond to the Fe_3Al and Ni_3Al phases, respectively.

Cases I–III refer to the Ni-deficit $Ni_{75-x}Fe_xAl_{25}$ alloys while IV and V relate to the Al-deficit $Ni_{75}Al_{25-x}Fe_x$ alloys. The computed functional dependences of $2\langle r_i \rangle$ on Fe concentration x for cases I–V, depicted in figure 9 by full straight lines, are compared with the observed (full symbols, this work; open circles, Pascarelli *et al* 1994) $r_{nn}(x)$ in figure 9; the broken straight lines through the $r_{nn}(x)$ data basically reflect an increase in the value of r_i^{Fe} in the 'as-prepared' and 'quenched' samples, as discussed later in the text. From such a comparison between theory and experiment, it is evident that cases I and V adequately describe the observed variations of r_{nn} with x in Ni-deficit and Al-deficit Ni_3Al alloys. Alternatively, it follows that Fe has *exclusive Ni-site preference* in Ni-deficit alloys whereas the occupancy of Fe in the Al (Ni) sites is $75 \pm 5\%$ ($25 \pm 5\%$) in the Al-deficit alloys.

This inference not only conforms well with the result of the channeling-enhanced microanalysis (Shindo *et al* 1988) that 70 ± 12 and $23 \pm 15\%$ Fe atoms occupy Ni sites in $Ni_{70}Fe_5Al_{25}$ and $Ni_{75}Al_{20}Fe_5$ alloys, respectively, but also with the observation, based on Fe K-edge extended x-ray absorption fine structure data (Pascarelli *et al* 1994), that 75% Fe atoms or more land on the Al sites in Al-poor alloys. Thus, in consonance with the recent theoretical prediction (Ruban and Skriver 1997), composition plays a crucial role in deciding the site preference of Fe. However, a good agreement between the calculated and observed variations of r_{nn} with x should not be taken to imply that the atomic size effects alone govern

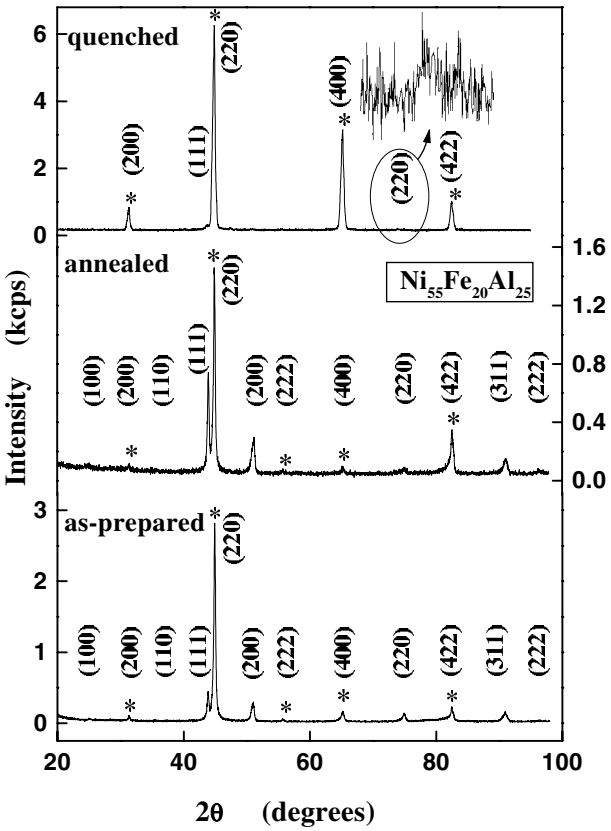

Figure 7. X-ray diffraction patterns for $Ni_{55}Fe_{20}Al_{25}$ samples with different thermal histories (see the text). This figure also presents an enlarged view of the (220) peaks of very weak intensity in the case of a 'quenched' $Ni_{55}Fe_{20}Al_{25}$ sample. The peaks with and without an asterisk correspond to the Fe_3Al and Ni_3Al phases, respectively.

the site preference of Fe, as is evident from the fact that the observed functional dependences of r_{nn} on x are not reproduced if the ionic radius of Al in Al metal, i.e. $r_i^{Al} = 1.43$ Å, is used in the above calculations. By using the value $r_i^{Al} = 1.31$ Å instead, due consideration has been given to other important factors such as the effective Ni–Al and Al–Al interactions (Ni–Ni pair interactions being the same as in the Ni metal) in the Ni_3Al compound.

A *steeper* but linear variation of r_{nn} with x in the 'quenched' and 'as-prepared' samples compared with that in their 'annealed' counterparts indicate that the *difference* in the ionic radii of Fe and Ni increases in the former samples, as is borne out by the following observation. The broken straight lines in figure 9, which closely reproduce $r_{nn}(x)$ data in the 'as-prepared' and 'quenched' samples, are obtained based on the assumption that r_i^{Fe} *increases* from 1.27 to 1.29 Å (the values of r_i^{Ni} and r_i^{Al} remaining the same as before) and that all the Fe atoms occupy the empty Ni sites left behind on the Ni sublattice after all the host Ni (Al) atoms have been accommodated on the Ni (Al) sublattice. An increase in the difference $r_i^{Fe} - r_i^{Ni}$ can be qualitatively understood as follows. The Fe_0 samples in the 'as-prepared' and 'quenched' states have a higher degree of site disorder (Semwal and Kaul 2002) than the 'annealed' one. In the quenched sample, in particular, 88 ± 2 $(12 \pm 2)\%$ of Ni or Al sites are occupied by Ni (Al) or Al (Ni) atoms (Semwal and Kaul 2002). The presence of Ni (Al) atoms on Al (Ni) sites

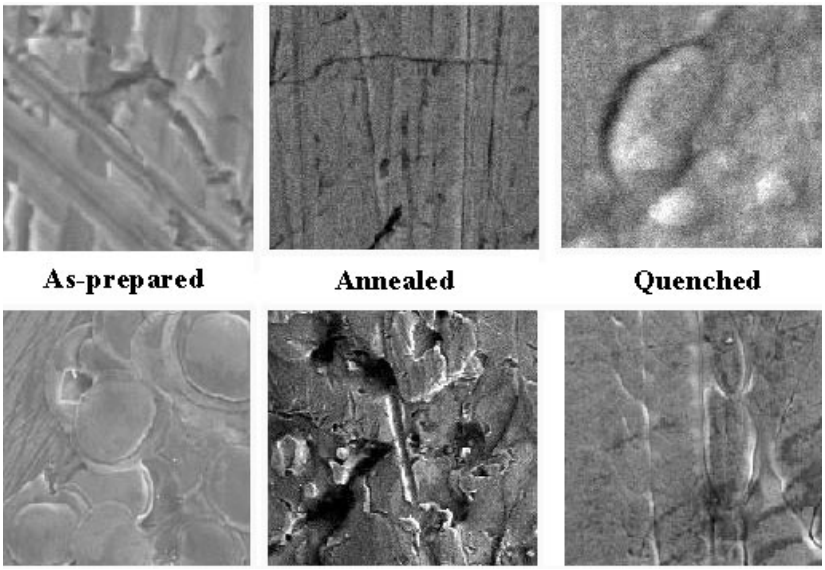

Figure 8. Scanning electron micrographs for 'as-prepared', 'annealed' and 'quenched' samples of $Ni_{75}Al_{25}$ (top panel) and $Ni_{55}Fe_{20}Al_{25}$ (bottom panel).

causes sizeable distortion in the Ni_3Al unit cells because of the large mismatch between the ionic radii of Ni and Al. This distortion gives rise to the satellite Bragg peaks in the diffraction pattern of the quenched Fe_0 sample (figures 3 and 4). Introduction of Fe progressively reduces this mismatch (and hence the lattice distortion) for the following reason. With increasing Fe concentration, more and more Fe atoms of larger (1.27 Å) ionic radius preferentially occupy the empty Ni sites and/or replace Ni atoms of smaller (1.245 Å) ionic radius at the Ni sites and the Ni atoms so dislodged from the Ni sites end up on the Al sublattice while Al atoms of much larger (1.31 Å) ionic radius displaced by Ni atoms at the Al sites appear on the Ni sites. In the process, increased 'mixing' of the Ni and Al sublattices takes place with the result that the lattice distortions are substantially reduced by increasing the Fe–Ni nearest-neighbour distance or, alternatively, the difference $r_i^{\mathrm{Fe}} - r_i^{\mathrm{Ni}}$ with x. The premise that in the *disordered* $Ni_{75-x}Fe_xAl_{25}$ alloys, Fe prefers a Ni sublattice to an Al sublattice is at variance with the theoretical prediction (Ruban and Skriver 1997) that the *entropy* increases the Al site preference for the ternary Fe addition in Ni-deficit alloys. The experimental observations, that the satellite Bragg peaks gradually disappear in the quenched samples and the brittleness decreases substantially in all the samples, are the consequences of a progressive diminution of the lattice distortion with increasing Fe concentration.

The existence of superstructure Bragg reflection peaks, besides the fundamental ones, basically reflects the presence of long-range atomic order in the sample in question. From the observed *integrated* intensities I_S and I_F of the Cu_3Au-type (100) or (110) superstructure (S) and the fcc-type (200) or (220) fundamental (F) Bragg reflection peaks in a given sample, the long-range order parameter $\boldsymbol{S}$ has been estimated using the relation (Warren 1978) $\boldsymbol{S}^2 = (I_S/I_F)_{sample} \times (I_F/I_S)_{S=1}$, where $(I_F/I_S)_{S=1}$ is the corresponding intensity ratio for the *fully ordered* Ni_3Al compound. In the absence of the experimental value of the quantity $(I_F/I_S)_{S=1}$, this ratio is calculated from the expression

$$(I_F/I_S)_{S=1} = \frac{\{X_{\mathrm{Ni}} f_{\mathrm{Ni}}(\theta) + X_{\mathrm{Al}} f_{\mathrm{Al}}(\theta)\}_F^2 \{L_P(\theta)\}_F \{\exp(-2M(\theta))\}_F}{\{f_{\mathrm{Ni}}(\theta) - f_{\mathrm{Al}}(\theta)\}_S^2 \{L_P(\theta)\}_S \{\exp(-2M(\theta))\}_S} \qquad (1)$$

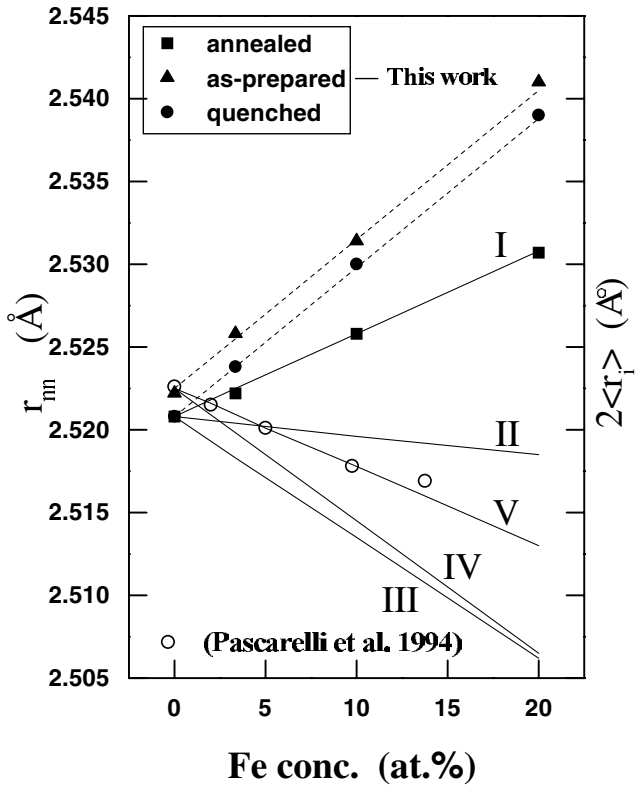

Figure 9. The nearest-neighbour interatomic distance, r_{nn}, as a function of the Fe concentration (x). In this figure, full symbols (open circles) represent the present (published; Pascarelli *et al* 1994) data while the full or broken straight lines through the data denote the theoretical $2\langle r_i\rangle(x)$ fits for various possibilities (including the cases I–V) of Fe site occupation considered in the text.

where X_{Ni} and X_{Al} are the concentrations of Ni and Al atoms in atomic fractions, f_{Ni} and f_{Al} are the atomic structure factors for Ni and Al, $L_P = (1 + \cos^2 2\theta)/\sin^2\theta\cos\theta$ is the Lorentz polarization factor, 2θ is the Bragg angle and $\exp(-2M)$ is the Debye–Waller factor with $M(\theta) = (3h^2/m_a k_B \Theta_D)\,\{(\phi(x)/x) + (1/4)\}(\sin\theta/\lambda)^2$, Debye integral $\phi(x) = (1/x)\int_0^x \xi\,\mathrm{d}\xi/(\mathrm{e}^{\xi} - 1)$, Debye temperature $= \Theta_D$, $x = \Theta_D/T$ and mass of the atom $= m_a$. In equation (1), the subscripts F and S refer, respectively, to the fundamental and superstructure reflections. The values of f_{Ni}, f_{Al}, L_P and $\exp(-2M)$ corresponding to the angles at which (100), (110) or (200), (220) superstructure or fundamental Bragg reflections in the fully ordered Ni_3Al compound occur (Grant 1957), are taken from the standard international tables (1959, 1962, 1967) and inserted into equation (1) to obtain the theoretical estimates for the ratio $[I_F^{(200)}/I_S^{(100)}]_{S=1}$ or $[I_F^{(220)}/I_S^{(110)}]_{S=1}$. The long-range order parameter is then calculated from the relations $S^2 = [I_S^{(100)}/I_F^{(200)}]_{\mathrm{meas}} \times [I_F^{(200)}/I_S^{(100)}]_{S=1}$ and $S^2 = [I_S^{(110)}/I_F^{(220)}]_{\mathrm{meas}} \times [I_F^{(220)}/I_S^{(110)}]_{S=1}$, using the measured (denoted by subscript 'meas') integrated intensity ratios of the (100), (200) and (110), (220) reflections for a given sample. The values of S, so obtained, are listed in table 2 and plotted against the Fe concentration in figure 10.

According to the general definition $S = (r - w)/(r + w)$ of the long-range (atomic) order parameter, where r and w represent the number of right atoms (e.g. Ni atoms on Ni sites or Al atoms on Al sites) and wrong atoms (e.g. Ni and/or Fe atoms on Al sites or Al and/or

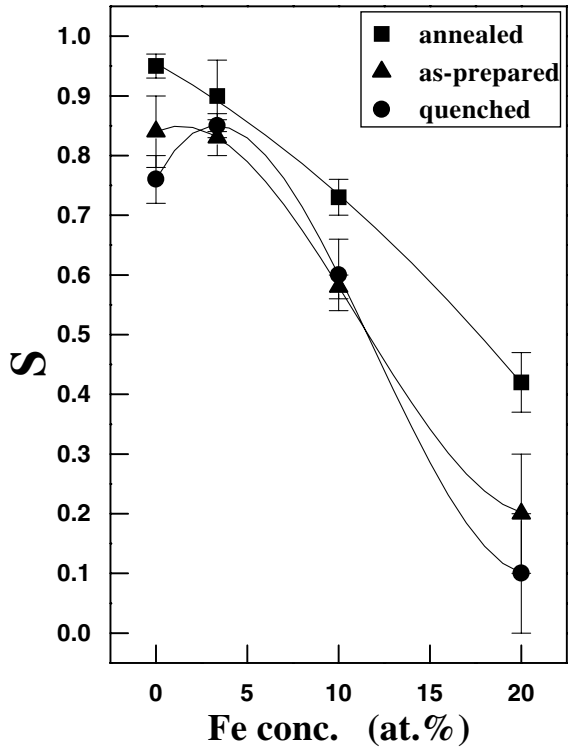

Figure 10. Long-range (atomic) order parameter as a function of Fe concentration for the samples with different thermal histories. The full symbols represent the data while the full curves through the data only serve as a guide to the eye.

Fe atoms on Ni sites), $\boldsymbol{S}$ attains its maximum value $\boldsymbol{S} = 1$ *only* for the *completely ordered* compound Ni_3Al when $w = 0$ and is bound to be *less than unity* when the Fe concentration is non-zero (since Fe atoms are the wrong atoms irrespective of whether they occupy Ni or Al sites). Thus, regardless of the sample thermal history and the site preference of Fe, $\boldsymbol{S}$ is expected to decrease monotonously with increasing Fe concentration (x), in agreement with the present observation (figure 10). The most striking feature of the above definition of the long-range order parameter is that it permits an accurate determination of the site occupation of the Ni and Al sublattices. To elucidate this point, we take the example of the 'as-prepared' and 'quenched' Fe_{10} samples for which the observed values of $\boldsymbol{S}$ are $\boldsymbol{S}_{\rm obs} = 0.58$ (2) and $\boldsymbol{S}_{\rm obs} = 0.60$ (6), respectively (table 2). For the Ni (Al) sublattice, $r + w = 75$ (25) and the value $\boldsymbol{S}_{\rm cal} = 0.6 = (r - w)/(r + w)$ yields $r - w = 45$ (15). It immediately follows that the number of right and wrong atoms on the Ni (Al) sublattice is $r = 60$ (20) and $w = 15$ (5), respectively. Considering that the actual composition of the alloy in question is $Ni_{65}Fe_{10}Al_{25}$ (table 1), the distribution of Ni, Fe, Al atoms on the Ni (Al) sublattice is 60, 10, 5 (5, 0, 20). In other words, 80, 13.3, 6.7% (20, 0, 80%) of Ni (Al) sites are occupied by Ni, Fe, Al atoms. The percentage (rounded off to the next significant digit) of Ni (Al) sites occupied by Ni, Fe, Al atoms in different samples, so obtained, are displayed in table 2. Consistent with the inferences drawn previously from the $r_{nn}(x)$ data (figure 9), the entries in table 2 assert that

(i) Fe has *exclusive Ni-site preference* particularly in the 'as-prepared' and 'quenched' samples; in the annealed samples, the *percentage* of Fe atoms occupying Ni (Al) sites reduces (increases) from about 90% (10) for Fe_5 to 65 (35) for Fe_{20}, and

Table 2. Long-range order parameter S and percentage Ni, Al site population.

			% Ni sites occupied by			% Al sites occupied by		
Sample	S_{obs}	S_{cal}	Ni	Fe	Al	Ni	Fe	Al
			As-prepared					
Fe_0	0.84(6)	0.84	92.0	0.0	8.0	8.0	0.0	92.0
Fe_5	0.83(3)	0.84	92.0	4.5	3.5	8.0	0.0	92.0
Fe_{10}	0.58(2)	0.60	80.0	13.0	7.0	20.0	0.0	80.0
Fe_{20}	0.20(10)	0.22	61.0	27.0	12.0	39.0	0.0	61.0
			Annealed					
Fe_0	0.95(2)	0.95	97.5	0.0	2.5	2.5	0.0	97.5
Fe_5	0.90(6)	0.88	94.0	4.0	2.0	4.5	1.5	94.0
Fe_{10}	0.73(3)	0.73	87.0	9.0	4.0	0.0	12.0	88.0
Fe_{20}	0.42(5)	0.46	73.0	17.5	9.5	0.0	28.0	72.0
			Quenched					
Fe_0	0.76(4)	0.76	88.0	0.0	12.0	12.0	0.0	88.0
Fe_5	0.85(2)	0.84	92.0	4.5	3.5	8.0	0.0	92.0
Fe_{10}	0.60(6)	0.60	80.0	13.0	7.0	20.0	0.0	80.0
Fe_{20}	0.10(10)	0.16	58.0	27.0	15.0	42.0	0.0	58.0

(ii) the effect of annealing is to *increase* the number of Ni (Al) atoms at the *expense* of Fe and Al (Ni) atoms on the Ni (Al) sublattice so much so that *all* the host Ni atoms reside on the Ni sublattice for Fe concentrations $\geqslant$10 at.%: consequently, for a given composition (Fe concentration x), S has a greatly enhanced value in the annealed sample as compared with that in the 'as-prepared' or 'quenched' counterpart (figure 10).

4. Summary and conclusion

With a view to resolve the issue of the site preference of the ternary Fe addition in $Ni_{75}Al_{25}$, an extensive investigation of structure, surface morphology and composition in Ni-deficit alloys with nominal composition $Ni_{70}Fe_5Al_{25}$, $Ni_{65}Fe_{10}Al_{25}$ and $Ni_{55}Fe_{20}Al_{25}$, 'prepared' in different states of site disorder, has been carried out by x-ray diffraction, scanning electron microscopy (SEM), x-ray fluorescence (EDAX) and inductively coupled plasma optical emission spectroscopy. Consistent with the results of SEM and EDAX studies, an elaborate analysis of the x-ray diffraction data reveals the following.

(I) Regardless of the sample thermal history, the nucleation of the Fe_3Al phase occurs at Fe concentrations as low as 3 at.% and this phase in the 'as-prepared' and 'quenched' samples grows at the expense of the Ni_3Al phase as the Fe concentration increases beyond 3 at.%, so much so that the Ni_3Al phase is relegated to a minor phase in the 'quenched' Fe_{20} sample.

(II) Fe has exclusive Ni-site preference, particularly in the 'as-prepared' and 'quenched' samples; in the 'annealed' sample, the percentage of Fe atoms occupying Ni (Al) sites reduces (increases) from about 90 (10) for Fe_5 to 65 (35) for Fe_{20}.

(III) Upon annealing, the number of Ni atoms increase at the expense of Fe and Al (Ni) atoms on the Ni (Al) sublattice such that all the host Ni atoms reside on the Ni sublattice for Fe concentrations $\geqslant$10 at.%.

As a result, annealing promotes the growth of the Ni_3Al phase at the cost of the Fe_3Al phase and, for a given Fe concentration, the long-range order parameter has a greatly enhanced value in the 'annealed' samples as compared with that in the 'as-prepared' or 'quenched' counterpart. Our observation that the brittleness reduces drastically with Fe concentration in Ni-deficit alloys agrees well with the previously reported result (Chiba *et al* 1990, 1991a, 1991b) that a substantial enhancement in the ductility occurs when the ternary addition *preferentially* substitutes Ni on the face-centred sites in the Ni_3Al compound. The present results on Ni-deficit alloys, together with the previously published (Shindo *et al* 1988, Pascarelli *et al* 1994 and Lawniczak-Jablonska *et al* 2000) data on Al-deficit alloys, provide strong experimental evidence for the theoretical prediction (Ruban and Skriver 1997) that, for a given sample's thermal history, the composition of the alloy essentially determines the site preference of the ternary Fe addition in that Fe has nearly *exclusive* Ni (Al) site preference in the Ni-deficit (Al-deficit) alloys and no discernible site preference in the equideficit (i.e. deficient to the same extent in Ni and Al with respect to the stoichiometric composition, $Ni_{75}Al_{25}$) alloys. From the experimental point of view, the conflicting reports about the site preference of Fe in the γ'-Ni_3Al phase in the literature could, therefore, be attributed to the fact that all the previous conclusions were drawn based on the nominal composition of the alloys which differed considerably from the actual composition. Our observation that Fe entirely occupies the Ni sites in the 'as-prepared' and 'quenched' samples, which possess a greater degree of site disorder than their 'annealed' counterparts, contradicts the theoretical result (Ruban and Skriver 1997) that entropy promotes Al site preference of Fe in alloys deficient in Ni.

Acknowledgment

The authors are grateful to the Department of Science and Technology, India, for support under grant D O no SP/S2/M-21/97.

References

Blavette D and Bostel A 1984 *Acta Metall.* **32** 811
Bohn H G, Schumacher R and Vianden R J 1987a *High Temperature Ordered Intermetallic Alloys II (MRS Symp. Proc. No 81)* ed N S Stoloff, C C Koch and C T Liu (Pittsburgh, PA: Materials Research Society) p 123
Bohn H G, Williams J W, Barret J H, Liu C T and Izumi O 1987b *High Temperature Ordered Intermetallic Alloys II (MRS Symp. Proc. No 81)* ed N S Stoloff, C C Koch, C T Liu and O Izumi (Pittsburgh, PA: Materials Research Society) p 127
Chiba A, Hanada S and Watanabe S 1990 *Mater. Trans. Japan Inst. Met.* **31** 824
Chiba A, Hanada S and Watanabe S 1991a *Acta Metall.* **39** 1799
Chiba A, Hanada S and Watanabe S 1991b *Scr. Metall. Mater.* **25** 303
Chiba A, Shindo D and Hanada S 1991 *Acta Metall. Mater.* **39** 13
Enomoto M and Harada H 1989 *Metall. Trans.* A **20** 649
Grant W 1957 *J. Met.* **9** 865
Hono K, Chiba A, Sakurai T and Hanada S 1992 *Acta Metall.* **40** 419
Inoue A, Tomioka H and Masumoto T 1983 *Metall. Trans.* A **14** 1367
Karg A V, Kornwalt D E and Kreige O H 1971 *J. Inst. Met.* **99** 301
Kriege O H and Baris J M 1969 *J. Less-Common Met.* **62** 195
Lawniczak-Jablonska K, Wojnecki R and Kachniarz J 2000 *J. Phys.: Condens. Matter* **12** 2333
Lin H and Pope D 1990 *J. Mater. Res.* **5** 763
Lin H, Seiberling L E, Lyman P E and Pope D P 1987 *High Temperature Ordered Intermetallic Alloys II (MRS Symp. Proc. No 81)* ed N S Stoloff, C C Koch and C T Liu (Pittsburgh, PA: Materials Research Society) p 117
Liu C T, White C L and Horton J A 1985 *Acta Metall.* **33** 213
Loomis W T, Freeman J W and Sponseller D L 1972 *Metall. Trans.* **3** 989
Machlin E S and Shao J 1977 *Scr. Metall.* **11** 859

Marty A, Bessiere M, Bley F, Calvayrac Y and Lefebure S 1990 *Acta Metall. Mater.* **38** 345
Marty A, Calvayrac Y, Guillet F and Cenedese P 1991 *Phys. Rev.* B **44** 640
Miller M K and Bentley J 1986 *J. Physique Coll.* **47** C7 463
Miller M K and Horton J A 1987 *High Temperature Ordered Intermetallic Alloys II (MRS Symp. Proc. No 81)* ed N S Stoloff, C C Koch, C T Liu and O Izumi (Pittsburgh, PA: Materials Research Society) p 117
Munroe P R and Baker I 1991 *J. Mater. Res.* **6** 943
Nelson J B and Riley D P 1945 *Proc. Phys. Soc.* **57** 160
Nicholls J R, Rawlings R D and Rees D 1977 *Acta Metall.* **25** 187
Numakura H, Yamada T, Koiwa M, Szabo I A, Hono K and Sakurai T 1993 *Defect Diffus. Forum* **95–98** 869
Ochiai S, Oya Y and Suzuki T 1984 *Acta Metall.* **32** 289
Pascarelli S, Boscherini F, Mobilio S, Lawniczak-Jablonska K and Kozubski R 1994 *Phys. Rev.* B **49** 984
Pope D P and Ezz S S 1984 *Int. Metall. Rev.* **29** 136
Rawlings R D and Staton-Bevan A E 1975 *J. Mater. Sci.* **10** 505
Ruban A V and Skriver H L 1997 *Phys. Rev.* B **55** 856
Semwal A and Kaul S N 2002 *J. Phys.: Condens. Matter* **14** 5829
Shindo D, Kikuchi M, Hirabayashi M, Hanada S and Izumi O 1988 *Trans. Japan Inst. Met.* **29** 956
Sluiter M H F and Kawazoe Y 1995 *Phys. Rev.* B **51** 4062
Suzuki T, Oya Y and Wee D M 1980 *Acta Metall.* **28** 301
Takasugi T and Izumi O 1985 *Acta Metall.* **33** 1259
Taylor A and Sinclair H 1945 *Proc. Phys. Soc.* **57** 126
Warren B E 1978 *X-Ray Diffraction* (London: Addison-Wesley)
Wolverton C and de Fontaine D 1994 *Phys. Rev.* B **49** 351
Wu Y P, Tso N C, Sanchez J M and Tien J K 1989 *Acta Metall.* **37** 2835
Xu J-H, Oguchi T and Freeman A J 1987 *Phys. Rev.* B **36** 4186